

Modeling mixed-mode oscillations of a slow-fast system near a singular tangency bifurcation

Ian Lizarraga^{1, a)}

School of Mathematics and Statistics, University of Sydney, Camperdown 2006, Australia

(Dated: 9 December 2019)

Identifying routes toward *mixed-mode oscillations* (MMOs)—periodic solutions consisting of large- and small-amplitude oscillations—is a burgeoning field of research in multiple-timescale dynamical systems. This paper concerns a recently catalogued bifurcation associated with the emergence of MMOs: a tangency of the unstable manifold of a unique equilibrium point with a repelling slow manifold. This tangency is fundamental because it functions as a ‘switch’ connecting different parts of the phase space via *slow manifolds*. Various invariant objects interact in complicated ways to produce various types of MMOs, but disentangling the relative significance of each object using analytical arguments remains a difficult problem. We take the optimistic view that this bifurcation provides a fertile ground for testing new numerical algorithms, with the ultimate goal of classifying the variety of MMOs appearing at a particular parameter value.

First, we explore some of the routes to complicated MMOs occurring just after this bifurcation. Using numerical bifurcation theory, we identify certain bifurcations in discrete return maps of the system at parameter values near to the tangency bifurcation, and translate these into statements about MMO transitions. These bifurcations do not sufficiently explain the existence of more elusive transitions and MMO types, so we are led to the second part of the analysis: we construct a new dynamical partition of the domain of two-dimensional return maps in the system. This construction relies upon topological conditions which are well-defined only when the parameter characterizing a timescale ratio in the dynamical system is sufficiently small. With the aid of this partition, we identify sets of unusual ‘medium’-amplitude MMOs which occur as fixed points of a return map, and we also give numerical evidence of a Smale-Birkhoff homoclinic orbit as a route to chaotic MMOs. This partition construction should be compared to the identification of ‘rotation sectors,’ which have been used to organize less-complicated return maps of more elementary singular bifurcations.

PACS numbers: 05.45.-a, 05.45.Ac

Keywords: Singular Hopf bifurcation, tangency bifurcation of invariant manifolds, mixed-mode oscillations

A typical three-dimensional slow-fast system can exhibit a startling variety of complicated periodic and chaotic motions as its parameters are varied. These might include classical scenarios arising in three-dimensional flows, such as Shilnikov bifurcations and period-doubling cascades. But there are also intricate interactions occurring between invariant manifolds (such as fixed points, periodic orbits, and (un)stable manifolds of these objects), and slow manifolds, which emerge when the characteristic ratio of timescales in the system is sufficiently small. These interactions herald entirely new and interesting solutions, such as mixed-mode oscillations.

A self-contained ‘singular’ bifurcation theory for these systems is not fully formed. In the meantime, a hybrid of numerical and geometric methods can be applied fruitfully to study their phase portraits.

In this paper, we study a particularly complicated tangency bifurcation of two-dimensional manifolds, which heralds the existence of mixed-mode oscillations. Our approach is to study

return maps defined on two-dimensional cross-sections. We also provide a new dynamical partition of these return maps. We argue that this partition is natural for studying these complicated two-dimensional returns, and may be used to illuminate similarly complicated bifurcation scenarios. As an application, we successfully classify several types of solutions. These include chaotic mixed-mode oscillations and ‘medium’-amplitude oscillations, which are not categorized neatly into the usual framework which counts ‘large’ versus ‘small’ loops.

I. INTRODUCTION

Mixed-mode oscillations (MMOs) are periodic solutions of a dynamical system containing large and small amplitude oscillations and a distinct separation between the two. These solutions may be characterized by their signatures, which are symbolic sequences of the form $L_1^{s_1} L_2^{s_2} \dots L_k^{s_k}$. This notation is used to indicate that a particular solution undergoes L_1 large oscillations, followed by s_1 small oscillations, followed by L_2 large oscillations, and so on. The distinction between ‘large’ and

^{a)}Electronic mail: ian.lizarraga@sydney.edu.au

‘small’ oscillations is dependent on the model. We also refer to nontrivial, aperiodic, bounded solutions as MMOs. These include solutions having arbitrarily long, nonrepeating signatures. Such MMOs may be chaotic.

The classification of routes to MMOs with complicated signatures as well as chaotic MMOs continues to garner interest. Global bifurcations of multiple-timescale (or simply *slow-fast*) dynamical systems are natural starting points in this direction.

We study slow-fast dynamical systems of the form

$$\begin{aligned}\varepsilon \dot{x} &= f(x, y, \varepsilon) \\ \dot{y} &= g(x, y, \varepsilon),\end{aligned}\quad (1)$$

where $x \in R^m$ is the *fast* variable, $y \in R^n$ is the *slow* variable, $\varepsilon > 0$ is the *singular perturbation parameter* that characterizes the ratio of the timescales, and f, g are sufficiently smooth. The *critical manifold* $C = \{f = 0\}$ is the manifold of equilibria of the fast subsystem defined by $\dot{x} = f(x, y, 0)$. When ε is sufficiently small, theorems of Fenichel¹ guarantee the existence of locally invariant *slow manifolds* that perturb from subsets of C where the equilibria are hyperbolic. We may also project the vector field $\dot{y} = g(x, y, 0)$ onto the tangent bundle TC . Away from folds of C , we may desingularize this projected vector field to define the *slow flow*. The desingularized slow flow is oriented to agree with the full vector field near stable equilibria of C . For sufficiently small values of ε , trajectories of the full system can be decomposed into segments lying on the slow manifolds near C together with fast jumps across branches of C . Trajectory segments lying near the slow manifolds converge to solutions of the slow flow as ε tends to 0.

In the case of two slow variables and one fast variable ($m = 1, n = 2$), C is two-dimensional and its folds form curves. Selected points on fold curves are called *folded singularities*. When the slow flow is two-dimensional we use the terms “folded node”, “folded focus”, and “folded saddle” to denote folded singularities of node-, focus-, and saddle-type, respectively. In analogy to classical bifurcation theory, folded saddle-nodes are folded singularities having a zero eigenvalue. These are classified according to their persistence as equilibria in the full system of equations; folded-saddle nodes of type II (FSNII) are true equilibria of the full system. At a *singular Hopf bifurcation*, a pair of eigenvalues of the linearization of the flow crosses the imaginary axis, and a small-amplitude periodic orbit is born at the bifurcation point. These are shown to occur generically at $O(\varepsilon)$ -distances from the FSNII in parameter space.²

Characterizing the behavior near a folded singularity has been the subject of intense study. In the case of a folded node, Benoît⁴ and Wechselberger⁵ observed that the maximum number of small oscillations made by a trajectory passing through the folded node region can be counted using the ratio of eigenvalues of the linearization near the folded node. Guckenheimer³ has also analyzed

the local flow maps and global return maps of normal forms exhibiting folded nodes and folded saddle-nodes, showing that such folded singularities can give rise to complex and chaotic behavior.

In a complementary direction, period-doubling cascades, torus bifurcations,² and more recently, Shilnikov homoclinic bifurcations⁷ have been shown to produce MMOs with complex signatures. Even so, the connection between these bifurcations and interactions of slow manifolds—which organize the global dynamics for small values of ε —remains poorly understood.

In this paper, we study a minimal example of a slow-fast three-dimensional system having a so-called “*S*-shaped” critical manifold. Parametric subfamilies of this dynamical system have served as important prototypical models of electrochemical oscillations.⁶

Our focus is a tangency bifurcation catalogued by Guckenheimer and Meerkamp.⁸ This tangency is important in the context of MMOs. In our system, there exist several mechanisms which can generate large and small oscillations: folded singularities and a saddle-focus equilibrium point are *local* mechanisms which generate small-amplitude twisting of orbits, and an *S*-shaped critical manifold allows repeated reinjection into these local regions via large-amplitude excursions. There is also a parametric family of stable periodic orbits emerging from the saddle-focus, which generate additional twists around the stable manifold of the saddle-focus.

Before the tangency has occurred, the small- and large-amplitude mechanisms are ‘disconnected’ by the basin of attraction of the periodic orbit, in the sense that nontrivial trajectories not lying in the basin of attraction escape to infinity. The tangency bifurcation suddenly ‘connects’ these mechanisms together via bands of trajectories, allowing MMOs to form (see II. Fig. 1). We expect that aspects of this geometric analysis will remain relevant for any sufficiently low-dimensional, smooth slow-fast system whose critical manifold is *S*-shaped in a local region of the phase space.

Another reason why this bifurcation is interesting is that there is an interplay of *several* local mechanisms which produce twisting behavior. The delicate analytic arguments used to study twists near isolated folded singularities, or near saddle-foci, do not easily generalize to produce an accurate global analysis. We are left with numerical approximation of return maps to illuminate key features of the bifurcation.

Due to strong phase space contraction towards *attracting* slow manifolds of the system, it is possible to approximate return maps on cleverly chosen cross-sections with one-dimensional maps on an interval. We show that such maps are characterized by wildly varying derivatives and nonzero-length gaps which may be characterized as escape sets, corresponding to orbits which lie in the basin of attraction of the stable periodic orbit. The fixed points of these maps correspond to MMOs of the full system; however, the one-dimensional approximation gives limited information about the types of MMOs that emerge.

To further understand how these large and small oscillations connect, we must turn to two-dimensional return maps defined on cross-sections near to the equilibrium point and folded singularity. We show that the return dynamics, although highly nonlinear with regions of immense stretching and contraction as well as escape regions, are nonetheless organized by the slow manifolds of the system, together with the stable manifold of the equilibrium point and the periodic orbit's basin of attraction.

Our goal is to understand transitions of small to large oscillations. This requires disentangling the relative influence of the folded singularity versus the saddle-focus. Our approach is to partition the domain of the return map depending not only on the number of small turns the corresponding trajectories make—a technique which has been used previously to draw ‘rotation sectors’ of return maps in other slow-fast problems—but also on the direction of the jump from the repelling slow manifold. We argue that this partition is able to accurately distinguish between the various small-amplitude mechanisms, which is a new step forward for slow-fast systems of this type. For example, we show that the small oscillations of trajectories jumping right are characteristic of twists due to a folded node, whereas small oscillations of trajectories jumping left spiral out along the unstable manifold of the saddle-focus. Trajectories jumping left or right also return to the cross-section very differently, giving us more confidence that this partition isn't spurious.

The remainder of this paper is organized as follows.

- In Sec. II, we define the three-dimensional slow-fast system and describe the dynamics near the tangency bifurcation at a broad level.
- In Sec. III, we define one-dimensional approximations to return maps and describe saddle-node bifurcations and period-doubling cascades of MMOs. We also describe the statistics of the return map at a parameter set within a chaotic window of the period-doubling sequence.
- In Sec. IV, we define a return map on a two-dimensional cross-section. We use the slow manifolds and the basin of attraction of the small-amplitude periodic orbit as guides to create a partition according to the turning behavior of trajectories with initial conditions on that cross-section. We define a symbolic map encoding the return dynamics of partition subsets, and use this to streamline the discussion by giving concrete constructions of MMOs with varying symbolic dynamics. We also identify a Smale-Birkhoff homoclinic orbit, giving rise to a full-shift over a finite set of symbols and return horseshoes. We give numerical evidence that this chaotic invariant set may be a chaotic attractor of the full system.

II. DEFINING THE TANGENCY BIFURCATION

We study the following three-dimensional flow:

$$\begin{aligned}\varepsilon\dot{x} &= y - x^2 - x^3 \\ \dot{y} &= z - x \\ \dot{z} &= -\nu - ax - by - cz,\end{aligned}\tag{2}$$

where x is the fast variable, y, z are the slow variables, and $\varepsilon, \nu, a, b, c$ are the system parameters. This system exhibits a singular Hopf bifurcation.^{2,9,10} The critical manifold is the S-shaped cubic surface $C = \{y = x^2 + x^3\}$ having two fold lines $L_0 := S \cap \{x = 0\}$ and $L_{-2/3} := S \cap \{x = -2/3\}$. When $\varepsilon > 0$ is sufficiently small, nonsingular portions of C perturb to families of slow manifolds: near the branches $S \cap \{x > 0\}$ (resp. $S \cap \{x < -2/3\}$), we obtain the *attracting slow manifolds* S_ε^{a+} (resp. S_ε^{a-}) and near the branch $S \cap \{-2/3 < x < 0\}$ we obtain the *repelling slow manifolds* S_ε^r . Nearby trajectories are exponentially attracted toward S_ε^\pm and exponentially repelled from S_ε^r . One derivation of these estimates uses the Fenichel normal form.¹¹ Within each family, these sheets are $O(-\exp(c/\varepsilon))$ close,^{11,12} so we refer to any member of a particular family as ‘the’ slow manifold. This convention should not cause confusion.

We focus on parameters where forward trajectories beginning on S_ε^{a+} interact with a ‘twist region’ near L_0 , a saddle-focus equilibrium point p_{eq} , or both. A folded singularity $n = (0, 0, 0) \in L_0$ centers this twist region. The saddle-focus p_{eq} has a two-dimensional unstable manifold W^u and a one-dimensional stable manifold W^s . This notation disguises the dependence of these manifolds on the parameters of the system.

A. Tangency bifurcation of S_ε^r with W^u

Guckenheimer and Meerkamp⁸ drew bifurcation diagrams of the system (2) in a two-dimensional slice of the parameter space defined by $\varepsilon = 0.01$, $b = -1$, and $c = 1$. Codimension-one tangencies of S_ε^r and W^u are represented in Fig. 5.1 of their paper by smooth curves (labeled T) in (ν, a) space. For fixed a and increasing ν , this tangency occurs after p_{eq} undergoes a supercritical Hopf bifurcation. A parametric family of stable limit cycles emerges from this bifurcation. Henceforth we refer to ‘the’ small-amplitude stable periodic orbit Γ to mean the corresponding member of this family at a particular parameter set, and $B(\Gamma)$ will refer to its basin of attraction. The two-dimensional stable manifolds of Γ interact with the other invariant manifolds of the system. We will show that $B(\Gamma)$ has a significant influence on the global returns of the system.

Fixing $a = -0.03$, the tangency occurs within the range $\nu \in [0.00647, 0.00648]$. The location of the tangency may be approximated by studying the asymptotics of orbits beginning on S_ε^{a+} . Fix a section $\Sigma_+ =$

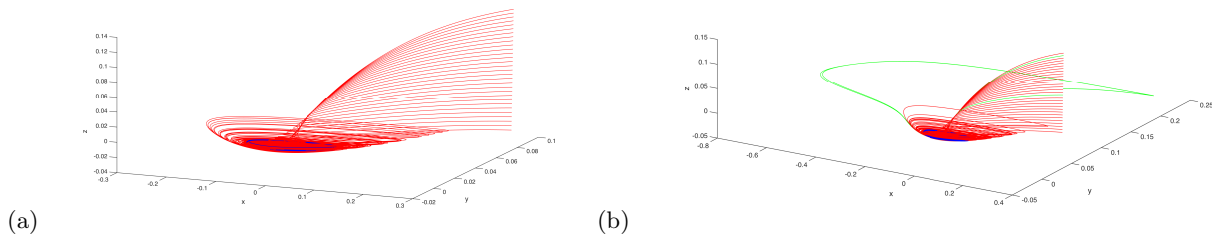


FIG. 1. Phase space (a) just before ($\nu = 0.00647$) and (b) just after ($\nu = 0.00648$) tangency bifurcation of W^u with S_ε^r . Thirty trajectories are initialized in a band on Σ_+ . Blue curve: small-amplitude stable periodic orbit Γ . Red curves: forward trajectories tending asymptotically to Γ without jumping to S_ε^- . Green curves: forward trajectories making a large-amplitude excursion before returning to Σ_+ . Remaining parameters are $\varepsilon = 0.01$, $a = -0.3$, $b = -1$, $c = 1$.

$S_\varepsilon^{a+} \cap \{x = 0.27\}$. Before the tangency occurs, trajectories lying on and sufficiently near W^u must either escape to infinity or asymptotically approach Γ ; these trajectories cannot jump to the attracting branches of the slow manifold, as they must first intersect S_ε^r before doing so. Trajectories beginning in Σ_+ first flow very close to p_{eq} . As shown in Fig. 1, these trajectories then leave the region close to W^u . Before the tangency, W^u forms a part of the boundary of $B(\Gamma)$. Therefore, all trajectories sufficiently high up on S_ε^{a+} must lie inside $B(\Gamma)$ (Fig. 1(a)).

After the tangency has occurred, W^u and S_ε^r will generically intersect transversely along isolated trajectories. These trajectories will bound sectors of trajectories that can now make large-amplitude passages. Trajectories within these sectors jump ‘to the left’ toward S_ε^- or ‘to the right’ toward S_ε^{a+} . Trajectories initialized in Σ_+ that leave neighborhoods of p_{eq} near these sectors contain *canards*, which are segments lying along S_ε^r . Examples of such trajectories are highlighted in green in Fig. 1. We can now establish a dichotomy between those trajectories in Σ_+ that immediately flow into a neighborhood of Γ and never leave, versus those that make a global return. In Fig. 1(b), only two of the thirty sample trajectories are able to make a global return. Near the boundaries of these subsets, trajectories can come arbitrarily close to Γ before escaping and making one large return. Note however that such trajectories might still lie inside $B(\Gamma)$, depending on where they return on Σ_+ . Such trajectories escape via large-amplitude excursions at most finitely many times before tending asymptotically to Γ . We now focus on the parameter regime where the tangency has already occurred. In Fig. 5.1 of the paper of Guckenheimer and Meerkamp, this corresponds to the region to the right of the T (manifold tangency) curve.

III. ONE DIMENSIONAL RETURN MAPS

The return map $R : \Sigma_+ \rightarrow \Sigma_+$ is well-approximated by a rank-one map on an interval, also denoted R . Our

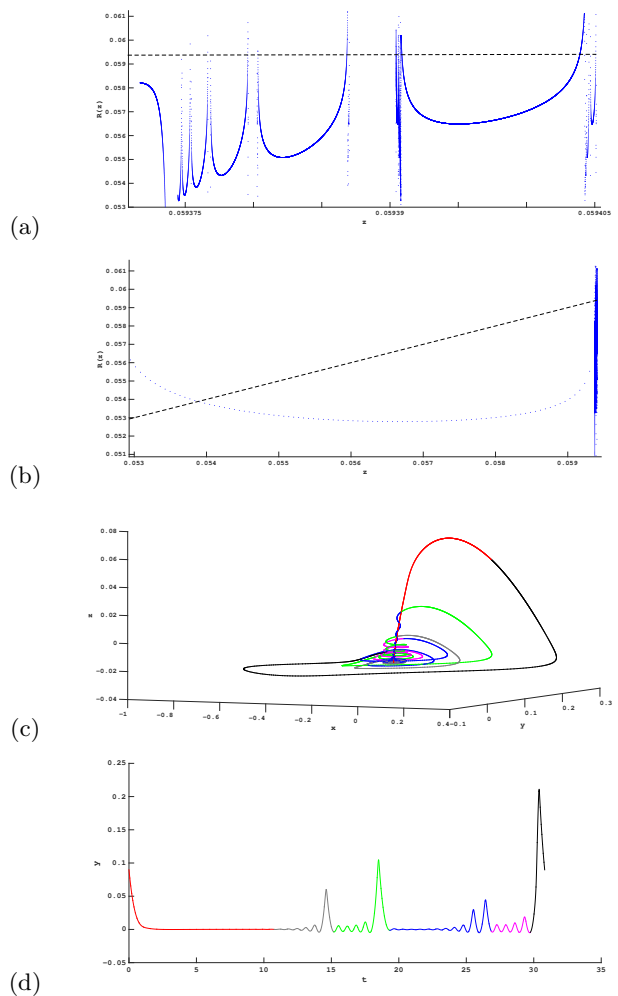


FIG. 2. (a-b) Subinterval of the return map $R : \Sigma_+ \rightarrow \Sigma_+$ of Eqs. (2) ((a) is a zoom-in of the right end of (b)). Dashed black line is the line of fixed points. (c) Periodic orbit corresponding to fixed point of R at $z \approx 0.05939079$. (d) Time series of the periodic orbit. The orbit is decomposed into red, gray, green, blue, magenta, and black segments (defined in Sec. III). Parameter set: $\nu \approx 0.00870134$, $a = -0.3$, $b = -1$, $c = 1$.

approach in studying the dynamics of R is similar to the analysis performed for return maps near folded nodes⁵ and folded saddle-nodes.^{3,13} In those cases, rotation sectors partitioning the domain of the return map are identified. These components, arising from the twisting that occurs near a folded singularity, classify trajectories according to the number of small turns they make.⁵

In the present case there is a folded singularity, a saddle-focus, and a small-amplitude periodic orbit; each of these local objects plays a role in the twisting of trajectories that enter neighborhoods of the fold curve L_0 . The remainder of this section carries out three tasks:

- first, we approximate the return map by a one-dimensional map on an interval and describe the typical dynamics of a trajectory (in the full system) corresponding to returns of this map;
- then, we demonstrate the existence of saddle-node and period-doubling bifurcations in this one-dimensional approximation and describe how these bifurcations relate to transitions of MMOs occurring in the full system; and
- finally, we describe a parameter set on which the return dynamics are well-approximated by a unimodal map having escape sets within the interval.

A. One-dimensional projection of mixed-mode oscillations

When Γ exists, the domain of the return map is now disconnected, with components separated by gaps of nonzero length (Fig. 2(a)). The gaps where R is undefined correspond to those trajectories beginning on S_ε^{a+} that asymptotically approach Γ without making a large-amplitude oscillation. Near the boundaries of the intervals where R is defined, the derivative changes rapidly within tiny intervals (Fig. 2(b)). These points arise from canard segments of trajectories resulting in a jump from S_ε^r to S_ε^{a+} and hence to Σ_+ . Fixing the parameters and iteratively refining successively smaller windows of initial conditions, this pattern of disconnected regions where the derivative changes rapidly repeats several times, certainly up to the double-precision arithmetic we use in our computations. One consequence of this structure is the existence of large numbers of unstable periodic orbits, defined by fixed points of R at which $|R'(z)| > 1$. This topological structure also appears to be robust to variations of the parameter ν .

This complicated structure arises from the interaction between $B(\Gamma)$, the twist region near the folded singularity and $W^{u,s}$. To illustrate this, consider an unstable fixed point $z \approx 0.05939079$ of the return map defined in Fig. 2(a). The corresponding unstable periodic orbit in the full system of equations is shown in Fig. 2(c)-(d). This orbit is approximately decomposed according to its interactions with the (un)stable manifolds of p_{eq} and the

slow manifolds. Here is one possible forward-time decomposition of this orbit:

- A segment (red) that begins on S_ε^{a+} and flows very close to p_{eq} by remaining near W^s ,
- a segment (gray) that leaves the region near p_{eq} along W^u , then jumping right from S^r to S_ε^{a+} ,
- a segment (green) that flows from S_ε^{a+} to S_ε^r , making small-amplitude oscillations while remaining a bounded distance away from p_{eq} , then jumping right from S_ε^r to S_ε^{a+} ,
- a segment (blue) that flows back down into the region near p_{eq} , making small oscillations around W^s , then jumping right from S_ε^r to S_ε^{a+} ,
- a segment (magenta) with similar dynamics to the green segment, making small-amplitude oscillations while remaining a bounded distance away from p_{eq} , then jumping right from S_ε^r to S_ε^{a+} , and
- a segment (black) making a large-amplitude excursion by jumping left to S_ε^{a-} , flowing to the fold $L_{-2/3}$, and then jumping to S_ε^{a+} .

A linearized flow map can be constructed^{14,15} in small neighborhoods of the saddle-focus p_{eq} , which can be used to count the number of small-amplitude oscillations contributed by orbit segments approaching the equilibrium point. However, the small-amplitude periodic orbit and the twist region produce additional twists, as observed in the green and magenta segments of the example above.

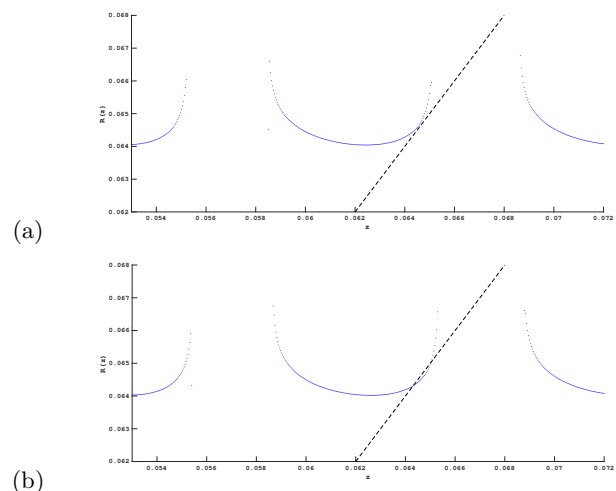


FIG. 3. Saddle-node bifurcation of periodic orbits in system (2). (a) $\nu = 0.00801$, (b) $\nu = 0.00802$. Dashed black line is the line of fixed points $\{z, z\}$. Remaining parameters: $a = -0.3, b = -1, c = 1$.

B. Bifurcations of MMOs: saddle-node and period-doubling

Fixed points of a return map defined on the section Σ_+ are interpreted in the full system as the locations of mixed-mode oscillations, formed from trajectories making one large-amplitude passage after interacting with the local mechanisms near L_0 . Similarly, periodic orbits of the (discrete) return map can be used to identify mixed-mode oscillations having more than one large-amplitude passage. We demonstrate common bifurcations associated with these invariant objects. First we locate a saddle-node bifurcation of periodic orbits, in which a pair of orbits coalesce and annihilate each other at a parameter value.

Fig. 3 demonstrates the existence of a fixed point $z = R(z)$ with unit derivative as ν is varied within the interval $[0.00801, 0.00802]$. Such a parameter set lies on a generically codimension one branch in the parameter space. Saddle-node bifurcations produce a stable-unstable pair of cycles in the full system (with identical signatures to the bifurcating orbit). Either of these may in turn undergo torus bifurcations and period-doubling cascades as a parameter is varied.

The beginning of a period-doubling cascade is identified in the return map R as ν is varied in the interval $[0.008685, 0.0087013]$ (Fig. 4a). Within this range, period-3, period-5, and period-6 windows are readily identifiable in Fig. 4(b). The local unimodality of the return map suggests that our (ν -parametrized) family of return maps share some universal properties with maps of the interval that exhibit period-doubling cascades,^{20,21} despite the nonlinearity at the right boundary of the interval observed in Fig. 2. This structure appears to be

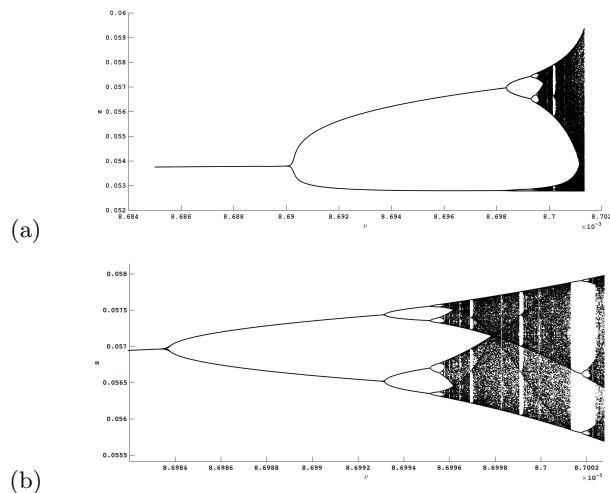


FIG. 4. (a) Period-doubling bifurcation sequence of the one-dimensional approximation of the return map $R : \Sigma_+ \rightarrow \Sigma_+$ as the parameter ν is varied from 0.008685 to 0.0087013. Remaining parameters: $a = -0.3$, $b = -1$, $c = 1$. (b) Magnification of upper branch of first period doubling cascade.

robust to small changes in the parameter ν .

We conclude by stressing that these bifurcations generate additional *large-amplitude* oscillations of MMOs (i.e. the transition is of the form $L_n^{s_n} \rightarrow (2L_n)^{s_n}$). In between period-doubling events, more small-amplitude twists may be generated, but a shortcoming of this one-dimensional analysis is that we cannot see where these intermediate bifurcations occur. The mechanism for producing small-amplitude oscillations will become clearer in part IV, when we study return maps defined on cross-sections nearer to p_{eq} and Γ .

C. Nontrivial aperiodic MMOs

We recall a classical result of unimodal dynamics for the quadratic family $f_a(x) = 1 - ax^2$ near the critical parameter $a = 2$, where $f_a : I \rightarrow I$ is defined on its invariant interval I (when $a = 2$, $I = [-1, 1]$). On positive measure sets of parameters near $a = 2$, the map f_a admits absolutely continuous invariant measures with respect to Lebesgue measure.²² These facts depend on the delicate interplay between stretching behavior away from neighborhoods of the critical point, together with recurrence to the arbitrarily small neighborhoods of the critical point as trajectories are ‘folded back’ under the action of f . This motivates our current objective: to lo-

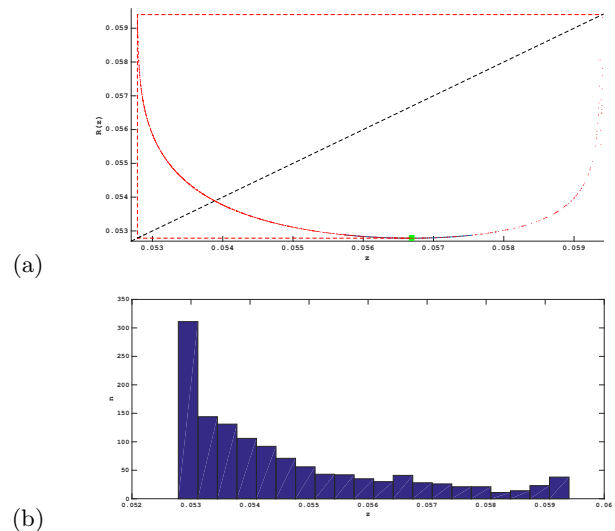


FIG. 5. (a) Forward trajectory (red points) of the critical point (green square) under the return map $R : \Sigma_+ \rightarrow \Sigma_+$. Red dashed lines indicate the cobweb diagram of the first two iterates of the trajectory to guide the eye. Black dashed line intersects the graph of R at fixed points. All 1284 forward iterates are plotted. The subsequent iterate lands outside the domain of R : the corresponding portion of the full trajectory of (2) tends asymptotically to Γ without returning to Σ_+ . (b) Distribution of points in the forward orbit of the critical point. Parameter set: $\nu \approx 0.00870134$, $a = -0.3$, $b = -1$, $c = 1$.

cate a parameter set for which (i) there exists a forward-invariant subset $\Sigma_u \subset \Sigma_+$ where $R : \Sigma_u \rightarrow \Sigma_u$ has exactly one critical point $c \in \Sigma_u$, and (ii) $R^2(c)$ is a fixed point of R .

It is difficult to locate a parameter set satisfying both (i) and (ii), but we can relax condition (i) to identify a parameter set where (i') R has the topology of Fig. 2 (i.e. is unimodal over a sufficiently large interval) and admits a critical point satisfying (ii). This parameter set is numerically approximated using a two-step bisection algorithm. First, a bisection method is used to approximate the critical point c by refining the region where R' first changes sign up to a fixed error tolerance 10^{-15} . Another bisection method is used to approximate the parameter value at which $|R^2(c) - R^3(c)|$ is minimized. This distance can be minimized to 2.5603×10^{-8} at the parameter set $(\nu, a, b, c) = (0.0087013381084, -0.3, -1, 1)$.

Fig. 5(a) depicts the forward trajectory of the critical point near the line of fixed points at this parameter value. The itinerary of c is finite, eventually landing in a subinterval of Σ_u where R is undefined. Even so, its forward orbit is unpredictable, sampling the interval $[R(c), R^2(c)]$ with a nontrivial transient density for 1284 iterates (Fig.5(b)). The length of the itinerary is extremely sensitive to tiny ($O(10^{-14})$) perturbations of the parameter b , reflecting the sensitive dependence of initial conditions in the selected parameter neighborhood. However, the distributions of the forward iterates appear to be more robust to small parameter changes: they are all similar to the distribution shown in Fig. 5(b).

IV. TWO-DIMENSIONAL RETURN MAPS

Fix a compact subset $\Sigma_0 \subset \{z = 0\}$ containing the first intersection (with orientation $\dot{z} > 0$) of W^s and such that $\Gamma \cap \Sigma_0 = \emptyset$, and let ϕ^t be the flow associated to the dynamical system, with $t \in \mathbb{R}$. We define the *immediate basin of attraction* $B_0 \subset B(\Gamma)$ of Γ as the set of points in $x \in \Sigma_0 \cap B(\Gamma)$ such that $\phi^{t>0}x \cap \Sigma_0 = \emptyset$, with ∂B_0 its boundary.

The forward return map $R : \Sigma_0 \rightarrow \Sigma_0$ is undefined on the subset B_0 , and points landing in B_0 under forward iterates of R ‘escape.’ We have the set inclusion $\phi^{t \geq 0}(\cup_{i=0}^{\infty} R^{-i}(B_0)) \subset B(\Gamma)$, and the j -th iterate of the return map R^j is defined only on the subset $\Sigma_0 - \cup_{i=0}^j R^{-i}(B_0)$. We abuse notation slightly and denote by S_ε^{a+} (resp. S_ε^r) the intersections of these slow manifolds with Σ_0 . We also refer to the intersection of S_ε^{a+} (resp. S_ε^r) with Σ_0 as the *attracting* (resp. *repelling*) *spiral* due to its distinctive shape (see Figure 6). The basin B_0 is sampled by the gray points in Fig. 6(a), accounting for the finite-length gaps in the one-dimensional return maps.

The slow manifolds intersect transversely. Segments of the attracting spiral can straddle both B_0 and the repelling spiral. In Fig. 6(b), we color initial conditions based on the maximum y -coordinate achieved by the cor-

responding trajectory before its return to Σ_0 . Exchange Lemma-type calculations imply that only thin bands of trajectories are able to remain close enough to S_ε^r to jump at an intermediate height. We choose the maximum value of the y -coordinate to approximately parametrize the length of the canards. This parametrization heavily favors trajectories jumping left (from S_ε^r to S_ε^{a-}) rather than right (from S_ε^r to S_ε^{a+}), since trajectories jumping left can only return to Σ_0 by first following S_ε^{a-} to a maximal height, and then jumping from $L_{-2/3}$ to S_ε^{a+} . In Figure 6, S_ε^r separates the blue and yellow regions, allowing us to distinguish trajectories turning right to S_ε^{a+} or left to S_ε^{a-} before returning to Σ_0 . This distinction will become useful in constructing our dynamical partition later. Summarizing, ∂B_0 and S_ε^r partition this section according to the behavior of orbits containing canards.

Trajectories beginning in Σ_0 either follow W^s closely and spiral out along W^u or remain a bounded distance away from both the equilibrium point and W^s , instead making small-amplitude oscillations consistent with a folded node.

The transition from one type of small-amplitude oscillation to the other depends continuously on the initial condition from W^s , which we now demonstrate with an example. Two initial conditions are chosen on a vertical line embedded in the section $\{z = 0\}$, having the property that the resulting trajectory jumps right from S_ε^r at an intermediate height before returning to the section with orientation $\dot{z} < 0$. These initial conditions are found by selecting points in Fig. 6(b) in the blue regions lying on a ray that extends outward from the center of the repelling spiral. The corresponding return trajectories are plotted in Fig. 7. The production of small-amplitude oscillations is dominated by the saddle-focus mechanism: in the example shown, the red orbit exhibits four oscillations before the (relatively) large-amplitude return, whereas the blue orbit exhibits seven oscillations. We can select trajectories with increasing numbers of small-amplitude oscillations by picking points closer to $W^s \cap \{z = 0\}$.

A complication in this analysis which we have ignored until now is that jumps at intermediate heights, which are clearly shown to occur in these examples, blur the distinction between ‘large’ and ‘small’ oscillations in a mixed-mode cycle. We will construct one such ‘medium’ amplitude MMO concretely in the next section. This makes a classification of trajectories based on signature less useful. Our forthcoming partition will instead classify orbits based on the number of turns and on a ‘jump direction,’ which will remove this ambiguity.

A. Dynamical partitions

We now study some of the possible concatenations of small-amplitude oscillation segments as seen in Fig. 7. The basis for determining allowed concatenations is to

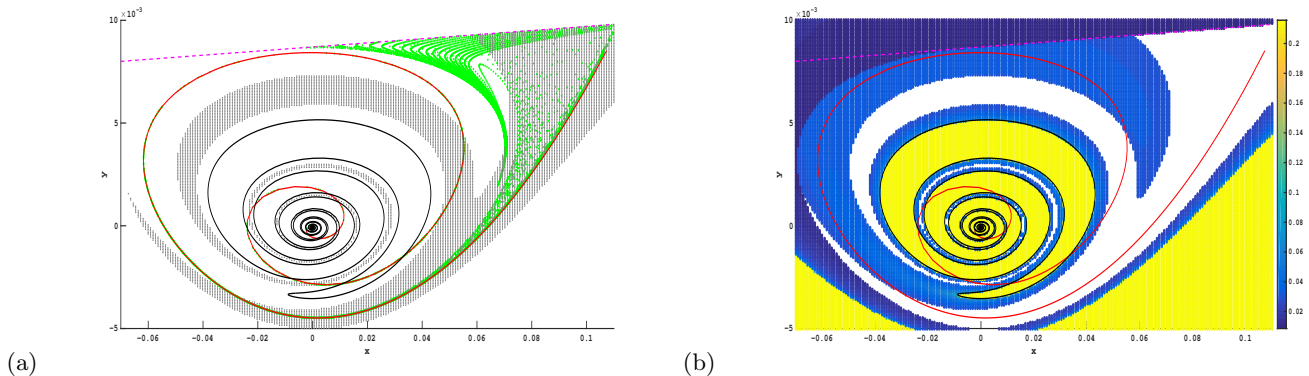


FIG. 6. (a) Geometry in the section $\Sigma_0 = \{(x, y, z) : x \in [-0.07, 0.11], y \in [-0.005, 0.01], z = 0\}$. Gray points sample the subset of Σ_0 whose corresponding forward trajectories tend to the stable periodic orbit without returning to Σ_0 . Green points denote the first forward return of the remaining points in Σ_0 with the orientation $\dot{z} < 0$. (b) Color plot of maximal height (y -coordinate) obtained by trajectories that return to Σ_0 as defined in (a). Cross-sections of S_ε^{a+} (red) and S_ε^r (black) at Σ_0 are shown, and the tangency of the vector field with Σ_0 (i.e. the set $\{ax + by = -\nu\}$) is given by the magenta dashed line. Parameter set: $\nu \approx 0.00870134$, $a = 0.01$, $b = -1$, $c = 1$.

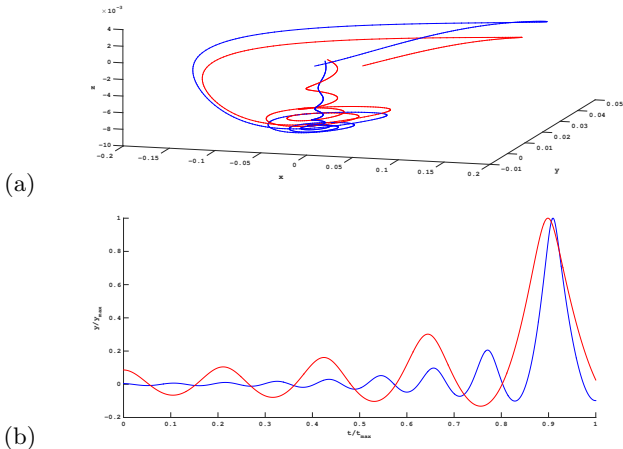


FIG. 7. (a) Two phase space trajectories beginning and ending on the section $\{z = 0\}$ with stopping condition $\dot{z} < 0$ and (b) the time series of the y -coordinates of each trajectory. To better compare qualitative differences between these orbit segments, stopping times and amplitudes are both rescaled to one. Initial conditions: blue, $(x, y, z) = (0.000553, 0.000201, 0)$; red, $(x, y, z) = (0.000553, 0.003065, 0)$. Parameter set: $\nu \approx 0.00870134$, $a = 0.01$, $b = -1$, $c = 1$.

partition the cross-section Σ_0 and then to study the images of these partition subsets under the forward return map. We gradually define this partition in stages:

- First, tangencies of the vector field with Σ_0 allow us to restrict to an invariant subset of the cross-section
- Then, we identify mixed-rank behavior in this subset which is intimately connected to the intersections of S_ε^{a+} with S_ε^r . This allows us to generate a

coarse partition.

- Finally, we define the winding number of a trajectory, which allows us to further refine this partition. Subsets in this refined partition therefore depend on both the turning of the trajectory with initial condition in Σ_0 as well as the location of this initial condition relative to S_ε^r .

Tangencies of the vector field with the cross-section are given by curves which partition the section into disconnected subsets. The subset that does not contain the attracting and repelling spirals is mapped with full rank to the remaining subset by the return map (Fig. 8(b)), allowing us to restrict our analysis to an invariant two-dimensional subset where the vector field is transverse everywhere. Mixed-rank behavior occurs in this subset, as shown in Fig. 8.

Note that the figures 8-12 are plotted at a slightly different parameter set from the earlier figures 6 and 7, whose parameter set was chosen to give a clearer picture of the main components of the return map. The main difference is that the line of vector field tangencies intersects a portion of the attracting spiral, but this does not affect the preceding arguments. Trajectories jumping left to S_ε^{a-} reach a greater maximal height (y -component) than the trajectories jumping right to S_ε^{a+} . The region is partitioned according to three criteria: their location with respect to the curve of tangency, and their location with respect to the repelling spiral (corresponding to left or right jumps), and their winding number, defined later in this section. See Fig. 8.

We can now state two significant results:

- *Mixed-rank dynamics.* As shown in Fig. 8(c)-(d), the red and blue regions collapse to S_ε^{a+} within one return. This includes those trajectories that return to the cross-section by first jumping right from S_ε^r

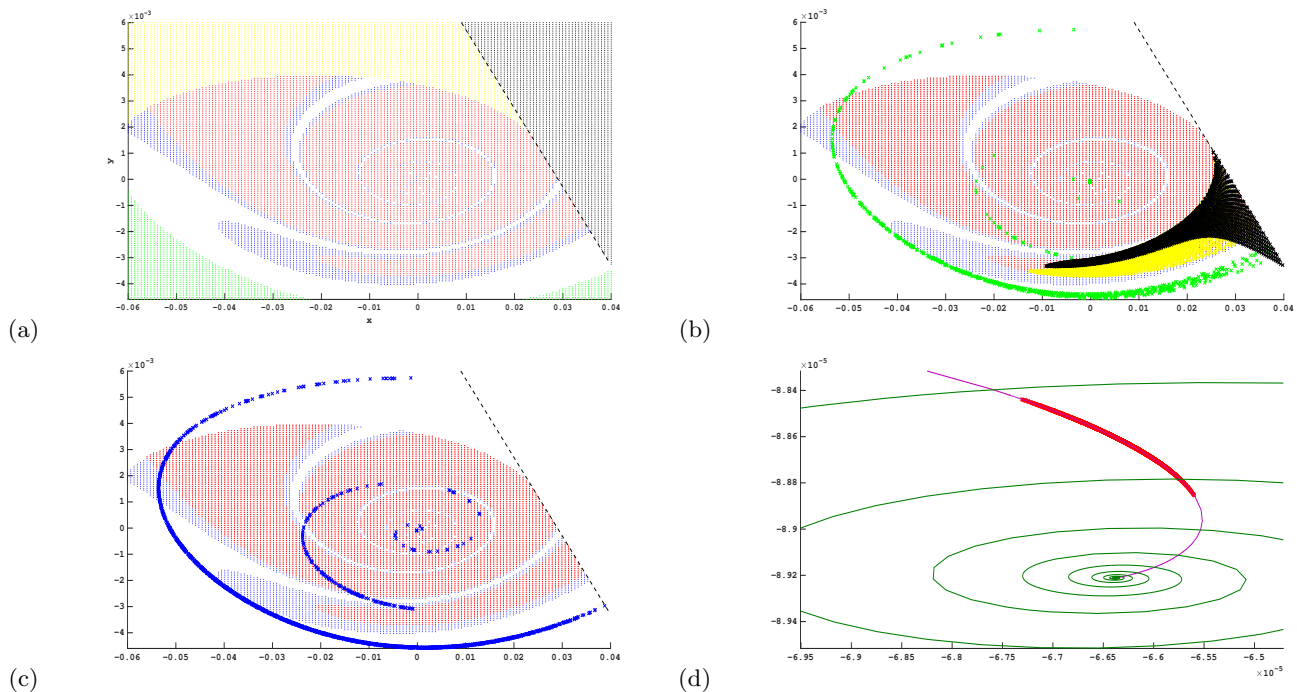


FIG. 8. (a) Partition of a compact subset of the cross-section Σ_0 . Black dashed line is the tangency of the vector field $\{\dot{z} = 0\}$, separating the subsets $\{z > 0\}$ (black points) and $\{z < 0\}$. Yellow (resp. green): points above (resp. below) the line $\{y = 0\}$ with winding number less than three. Red (resp. blue): points whose forward trajectories reach a maximal height greater than (resp. less than) 0.18 and have winding number three or greater. (b) Overlay of red and blue subsets of domain (points) with images of yellow, green, and black subsets (crosses). (c) Overlay of red and blue subsets of domain (points) with the image of the blue subset (crosses). (d) Overlay of attracting spiral (magenta), repelling spiral (dark green), and image of red subset (crosses). Note the change in scale of the final figure. Generated from a 500×500 grid of initial conditions beginning on Σ_0 . Parameter set: $\nu \approx 0.00870134$, $a = -0.3$, $b = -1$, $c = 1$.

to S_ε^{a+} at an intermediate height. Fig. 8(b) shows that the yellow subset returns immediately to this low-rank region. The green subset returns either to the low-rank region or to the yellow region. But note that it does not intersect its image, and furthermore, it intersects the yellow region on a portion of the attracting spiral. Therefore, after at most two returns the dynamics of the points beginning in Σ_0 (and which did not map to B_0) is characterized by the dynamics on the attracting spiral.

- *Trajectories jumping left or right return differently.* Those trajectories jumping left to S_ε^{a-} return to a tiny segment very close to the center of the S_ε^{a+} , as shown in Fig. 8(d). In contrast, the trajectories jumping right sample the entire spiral of S_ε^{a+} , as shown in Fig. 8(c). Thus, multiple intermediate-height jumps to the right are a necessary ingredient in concatenating small- and medium-amplitude oscillations (arising from right jumps) between large-amplitude excursions (arising from left jumps).

We now construct a dynamical partition of the cross-section. Let s and u denote a stable and unstable eigenvector, respectively, of the linearization of the flow at p_{eq} . Then consider a cylindrical coordinate system with basis

(u, s, n) centered at p_{eq} , where $n = u \times s$. The *winding* of a given trajectory is the cumulative angular rotation (divided by 2π) of the projection of the trajectory onto the (u, n) -plane. The *winding number* (or simply *number of turns*) of a trajectory is the integer part of the winding.

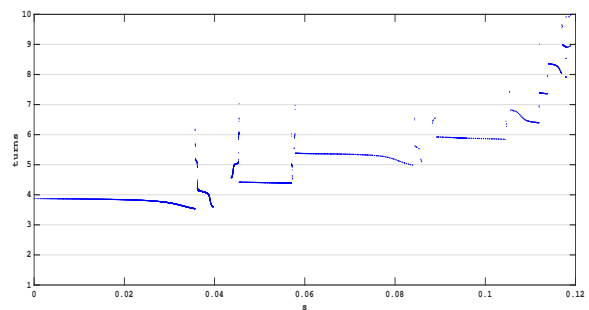


FIG. 9. Winding of the attracting spiral as a function of its parametrization by arclength. The starting point $s = 0$ is chosen close to the tangency. Positive values of s track the spiral as it turns inward. Parameter set: $\nu \approx 0.00870134$, $a = -0.3$, $b = -1$, $c = 1$.

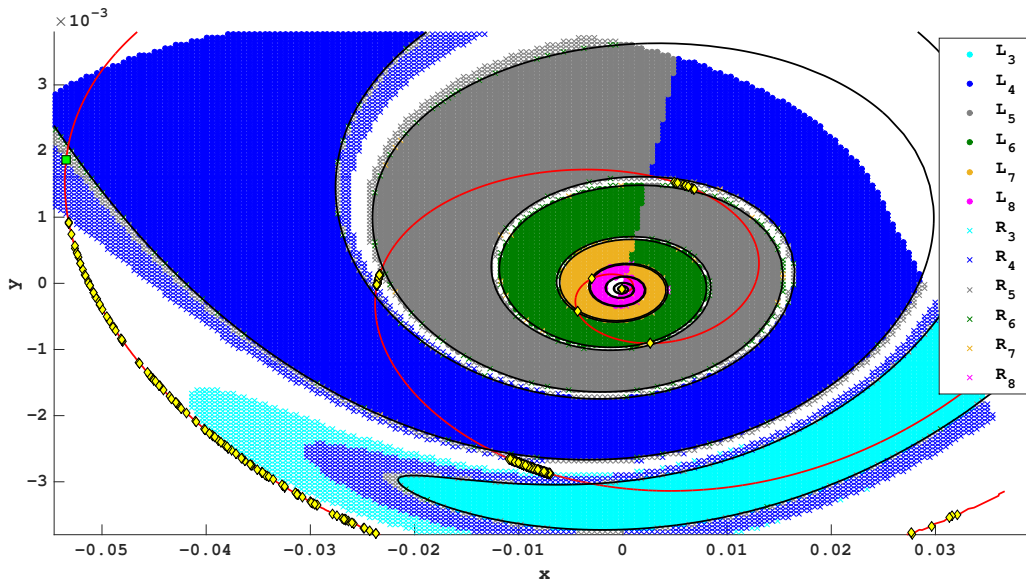


FIG. 10. Partition of the section $\Sigma_0 = \{z = 0\}$ according to number of turns made by corresponding trajectories as well as whether the trajectories turn left or right from S_ε^r . Left-turning trajectories are plotted with dots and right-turning trajectories are plotted with crosses. Color definitions: teal, 3 turns; blue, 4 turns; gray, 5 turns; green, 6 turns; gold, 7 turns; magenta, 8 turns. The slow manifolds S_ε^{a+} (red curve) and S_ε^r (black curve) and the saddle-point defined in Figure 11 (green square) are also shown. Yellow diamonds: final intersections of trajectories starting from a 20×20 grid of initial conditions beginning on Σ_0 , which exhibit between 4 and 35 returns before tending asymptotically to Γ . Parameter set: $\nu \approx 0.00870134$, $a = -0.3$, $b = -1$, $c = 1$.

The cumulative angular rotation depends on both the initial and stopping condition of the trajectory, which in turn depend on the section used. Close to p_{eq} , the winding of a trajectory measures winding around W^s . This is desirable since most of the rotation occurs as trajectories enter small neighborhoods of p_{eq} by winding around W^s .

If Fig. 9, we study the winding on a connected subset of the attracting spiral. On this connected subset we may parametrize the spiral by its arclength. The number of turns increases by approximately one whenever S_ε^{a+} intersects S_ε^r twice (these intersections occur in pairs since they correspond to bands of trajectories on S_ε^{a+} which leave the region by jumping left to S_ε^{a-}). In between these intersections, there are gaps corresponding to regions where S_ε^{a+} intersects B_0 .

As shown in Fig. 10, sets in the partition are defined according to each trajectory's winding number and jump direction. This partition uses the attracting and repelling spirals as a guide; small rectangles straddling the attracting spiral are contracted strongly transverse to the spiral and stretched along the attracting spiral, giving the dynamics a hyperbolic structure. In the next section we will compute a transverse homoclinic orbit, where this extreme contraction and expansion is shown explicitly.

B. Symbolic maps

We restrict ourselves to a subset $S \subset \Sigma_0$ where returns are close to rank one (i.e. the union of red and blue regions in Fig. 8(a)). Let $L_n \subset S$ (resp. $R_n \subset S$) denote points whose forward trajectories make n turns before jumping left to S_ε^{a-} (resp. right to S_ε^{a+}). Then define $L_{tot} = \cup_{n=0}^{\infty} L_n$ and $R_{tot} = \cup_{n=0}^{\infty} R_n$. The collection $\mathcal{P} = \{L_i, R_j\}_{i,j=1}^{\infty}$ partitions S . We clarify the following ambiguity: the newly-defined symbols L_i are unrelated to the large-amplitude oscillation notation in the definition of an MMO signature (eg. $L_i^{s_i}$).

For a collection of sets \mathcal{A} , let $\sigma(\mathcal{A})$ denote the set of all finite or infinite one-sided symbolic sequences $x = x_0x_1x_2\cdots$ with $x_i \in \mathcal{A}$. We can assign to each $x \in S$ a symbolic sequence in $\sigma(\mathcal{P} \cup \{S^c, B_0\})$, also labeled x . This sequence is constructed using the return map: $x = \{x_i\}$ is defined by $x_i = \iota(R^i(x))$, where $\iota: \Sigma_0 \rightarrow \mathcal{P} \cup \{B_0, S^c\}$ is the natural inclusion map. We allow finite sequences since R is undefined over B_0 . A portion of the partition is depicted in Fig. 10.

The results in Figs. 8 and 10 and the definition of B_0 constrain the allowed symbolic sequences:

- *Blocks containing S^c .* $R(S^c) \subset S$ (Fig. 8(b)).
- *Allowable symbols following R_i .* The following intersections with $R(R_{tot})$ are nonempty: $R(R_{tot}) \cap S_\varepsilon^{a+} \cap L_i \neq \emptyset$ and

$R(R_{tot}) \cap S_\varepsilon^{a+} \cap R_j \neq \emptyset$
whenever $L_i, R_j \neq \emptyset$ (Figs. 8(c) and 10).

- *Allowable symbols following L_i .* There exists a sufficiently large integer N with $R(L_{tot}) \subset S_\varepsilon^{a+} \cap (\cup_{n \geq N} L_n \cup R_n \cup B_0)$ (Figs. 8(d) and 10).
- *Finite symbol sequences.* The set of finite sequences are precisely those containing and ending in B_0 (yellow points in Fig. 10).

The subset S^c intersects the image of R_{tot} nontrivially. The first result implies the symbolic sequence of a point $x \in S$ whose forward returns leave the subset S must contain the block

$$x_{n_j-1} S^c x_{n_j},$$

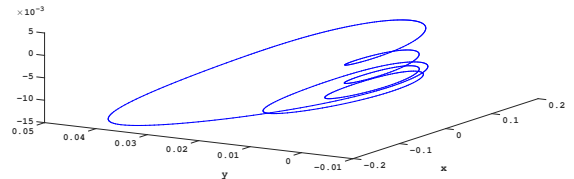
where the index n_j is defined by the j -th instance when the orbit leaves S and $x_{n_j-1} \in \mathcal{P}$. Our numerical results allow us to further constrain the allowed symbols of x_{n_j} . For the parameter set we used, the subset $R(S^c \cap S_\varepsilon^{a+})$ nontrivially intersects subsets of $\mathcal{P} \cup \{B_0\}$ only in the sub-collection $\mathcal{P}_c = \{L_3, L_4, L_5, R_3, R_4, R_5, B_0\}$. The portion of the attracting spiral which lies outside S is a subset of the region of Σ_0 where R has full rank. Therefore, the image of this portion of the attracting spiral is well-approximated by a curve segment lying inside the region sampled by the yellow and black points shown in Fig. 8(b). Therefore $x_{n_j} \in \mathcal{P}_c$ whenever n_j is defined.

The second result implies that for any integer $n \geq 1$, the block $L_n \alpha_m$ (where $\alpha \in \{L, R\}$) is impossible when $m < N$, since $R(L_n)$ is either B_0 or $\alpha_{m \geq N}$. For the parameter set used in Fig. 10, our calculations suggest $N \geq 13$. The third result reminds us that only right-jumping trajectories are able to sample the entire attracting spiral.

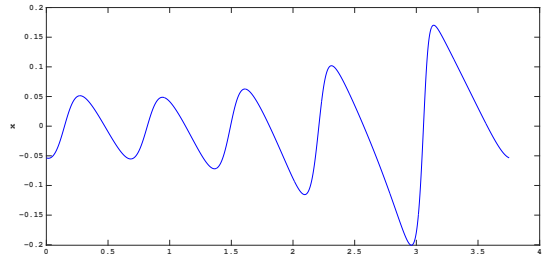
The second and third results then imply that blocks of type $R_i L_j$ or $R_i R_j$ are necessarily present in the symbolic sequences of orbits which concatenate small-amplitude oscillations with medium-amplitude oscillations as shown in Fig. 7, since medium-amplitude oscillations arise precisely from those points on Σ_0 whose forward trajectories remain bounded away from the saddle-focus (i.e. those points in Σ_0 sufficiently far from the intersection of W^s with Σ_0) and jump right. These results also imply that forward-invariant subsets lie inside the intersection of S_ε^{a+} with Σ_0 . In terms of the full system, it follows that the trajectories corresponding to these points each contain segments which lie within a sheet of S_ε^{a+} .

In view of the last result, for each $i \geq 1$ define the i -th *escape subset* E_i to be the set of length- i sequences ending in B_0 . Note that E_i contains the symbol sequences of the points in $R^{-(i-1)}(B_0)$. Escape rates of typical initial conditions in Σ_0 are studied in detail in the following section. The next section provides a concrete numerical example of a point in E_n , where n is at least 1284.

Let us summarize the main results of the symbolic dynamics. Points beginning on Σ_0 are identified with one of the following three types of one-sided symbolic sequences:



(a)



(b)

FIG. 11. (a) Mixed-mode oscillation in phase space corresponding to the saddle point $p \approx (-0.053438, 0.001873)$ of the return map defined on $\Sigma_0 = \{z = 0\}$ and (b) the time series of its x -component. Parameter set: $\nu \approx 0.00870134$, $a = -0.3$, $b = -1$, $c = 1$.

- Sequences ending in B_0 (tending asymptotically close to Γ)
- Sequences with an infinitely repeating finite block (periodic MMOs)
- Infinitely long, nonrepeating sequences (nontrivial, aperiodic MMOs).

C. Case study: Symbolic dynamics near a saddle-point and medium-amplitude oscillations

The structure of the invariant sets and escape sets of the two-dimensional return map is related to the intersection of the basin of attraction of the small-amplitude stable periodic orbit with Σ_0 . We begin by studying two types of invariant sets: fixed points and transverse homoclinic orbits.

Certain invariant sets of the map may be used to construct open sets of points all sharing the same initial block in their symbolic sequence. We briefly describe how the simplest kind of invariant set—a fixed point—implies that neighborhoods of points must have identical initial sequences of oscillations. In Fig. 11 we plot the saddle-type MMO corresponding to a saddle equilibrium point p , whose location in the section $\{z = 0\}$ is plotted in Figs. 10 and 12. According to Fig. 10, p has symbolic sequence $R_5 R_5 R_5 \dots$, in agreement with the time-series shown in Fig. 11(b). Observe that the fixed-point is sufficiently far away from W^s (the stable manifold of the saddle-focus) that the oscillations of the corresponding periodic orbit do not clearly arise from small winding

near p_{eq} . Furthermore, the dynamics in small neighborhoods of p are described by the linearization of the map R near p . This implies that small neighborhoods of p consist of points with initial symbolic blocks of R_5 , where the length of this initial block can be as large as desired. We can relax the condition that this be the initial block by instead considering preimages of these neighborhoods.

From this case study we observe that arbitrarily long chains of oscillations of varying sizes can be constructed using immediate neighborhoods of fixed points, periodic points, and other invariant sets lying in $S_\varepsilon^{a+} \cap \{z = 0\}$. These in turn correspond to complicated invariant sets in the full three-dimensional system. Consequently, the maximum number of oscillations produced by a periodic orbit having one large-amplitude return can be very large at a given parameter value, depending on the number of maximum possible returns to sections in the region containing these local mechanisms. This situation should be compared to earlier studies of folded-nodes, in which trajectories with a given number of small-amplitude oscillations can be classified,⁵ and the Shilnikov bifurcation in slow-fast systems, in which trajectories have unbounded numbers of small-amplitude oscillations as they approach the homoclinic orbit.⁷

D. Structure of invariant and escape sets

The return map R strongly contracts two-dimensional subsets of the cross-section to approximately one-dimensional subsets of S_ε^{a+} . Subsequent returns act on S_ε^{a+} by stretching and folding multiple times, before finally contracting strongly onto S_ε^{a+} again. Chaotic invariant sets and horseshoes of the two-dimensional return map must clearly be very degenerate. We now explore the structure of these invariant sets.

Let U be a small neighborhood of the saddle fixed point p that we located in the previous section. In Fig. 12 we plot U , $R(U)$, $U \cap R^{-1}(U)$, and $W^s(p)$ on the section Σ_0 . The image $R(U)$ is a nearly one-dimensional subset of S_ε^{a+} and the preimage is a thin strip which appears to be foliated by curves tangent to S_ε^r . The subsets $R(U)$ and $R^{-1}(U)$ contain portions of $W^u(p)$ and $W^s(p)$, respectively. The transversal intersection of $R(U)$ with $W^s(p)$ is also indicated in this figure.

Accurately computing R^{-1} is challenging. Trajectories which begin on the section and approach the attracting slow manifolds $S_\varepsilon^{a\pm}$ in reverse time are strongly separated, analogous to the scenario where pairs of trajectories in forward time are strongly separated by S_ε^r . This extreme numerical instability means that trajectories starting on the section and integrated backward in time typically become unbounded. In order to compute $W^s(p)$, we instead compute orbits in forward time and recast this as a boundary value problem, with initial conditions beginning in a line on the section and ending ‘at’ p . Beginning with a point y_0 along $W^s(p)$, we construct a sequence $\{y_0, y_1, \dots\}$ along $W^s(p)$ as follows.

(C1) *Prediction step.* Let $w_i = y_{i-1} + hv_i$, where h is a fixed step-size and v_i is a numerically approximated tangent vector to $W^s(p)$ at y_{i-1} .

(C2) *Correction step.* Construct a line segment L_i of initial conditions perpendicular to v_i . Use a bisection method to locate a point $y_i \in L_i$ such that $|R(y_i) - p| < \varepsilon$, where ε is a prespecified tolerance.

The relevant branch of $W^s(p)$ which intersects $R(U)$ lies inside the nearly singular region of the return map, so the segment L_i can be chosen small enough that $R(L_i)$ is approximately a segment of S_ε^{a+} which straddles p . This justifies our correction step above.

It is usually not sufficient to assert the existence of a transverse homoclinic orbit from the intersection of the image sets. But in the present case, these structures are organized by the slow manifolds S_ε^{a+} and S_ε^r . The strong contraction onto S_ε^{a+} in forward time implies that the discrete orbits comprising $W^u(p)$ must also lie along this slow manifold. The unstable manifold $W^u(p)$ lies inside a member of the $O(\exp(-c/\varepsilon))$ -close family which comprises S_ε^{a+} , so the forward images serve as good proxies for subsets of $W^u(p)$ itself. On the other hand, when U is sufficiently small, its preimage $R^{-1}(U)$ appears to be foliated by a family of curves tangent to S_ε^r , such that one of the curves contains $W^s(p)$ itself.

The Smale-Birkhoff homoclinic theorem^{16,17} then implies that there exists a hyperbolic invariant subset on which the dynamics is conjugate to a subshift of finite type. Fixed points lie in S_ε^{a+} due to strong contraction, but they need not lie in S_ε^r . We end this result by commenting on the apparent degeneracy of the two-dimensional sets U , $R(U)$, and $R^{-1}(U)$. A classical proof of the Smale-Birkhoff theorem uses a set $V = R^k(U) \cap R^{-m}(U)$ (with $k, m > 0$ chosen such that V is nonempty) as the basis for constructing the Markov partition on which the shift is defined.¹⁸ Here, V is well-approximated by a curve segment.

A natural question is whether this hyperbolic invariant set is indeed a chaotic attractor. It is difficult to conclusively decide set-invariance with finite-time computations. This difficulty is made clear in Fig. 12(b), where we study the eventual fate of a grid of initial conditions beginning on Σ_0 . This figure shows that even after a long integration time of $t = 600$, most initial conditions in B_0^c are able to return repeatedly to Σ_0 . However, it may simply be that the measure of $(R^{-n}(B_0))^c$ decays extremely slowly to 0 as n tends to infinity.

Nonetheless, we can recover some comparisons to well-studied maps which have escape subsets and hyperbolic behavior. Known results on escape rates of expansive maps suggest that the probability that a typical point does not escape after n returns decreases as c^{-n} for some positive constant c .¹⁹ Returning briefly to the section Σ_+ , define the function $E : \Sigma_+ \rightarrow \{0, 1, 2, \dots\} \cup \{\infty\}$ by $E(x) = n$ if n is the maximum integer for which $R^n(x)$ is defined (i.e. $R^n(x) \in B_0$) and $E(x) = \infty$ if $R^n(x)$ is defined for all n .

In Fig. 12(c) we compute $P(E(x) \leq n)$ vs. n for 10^4

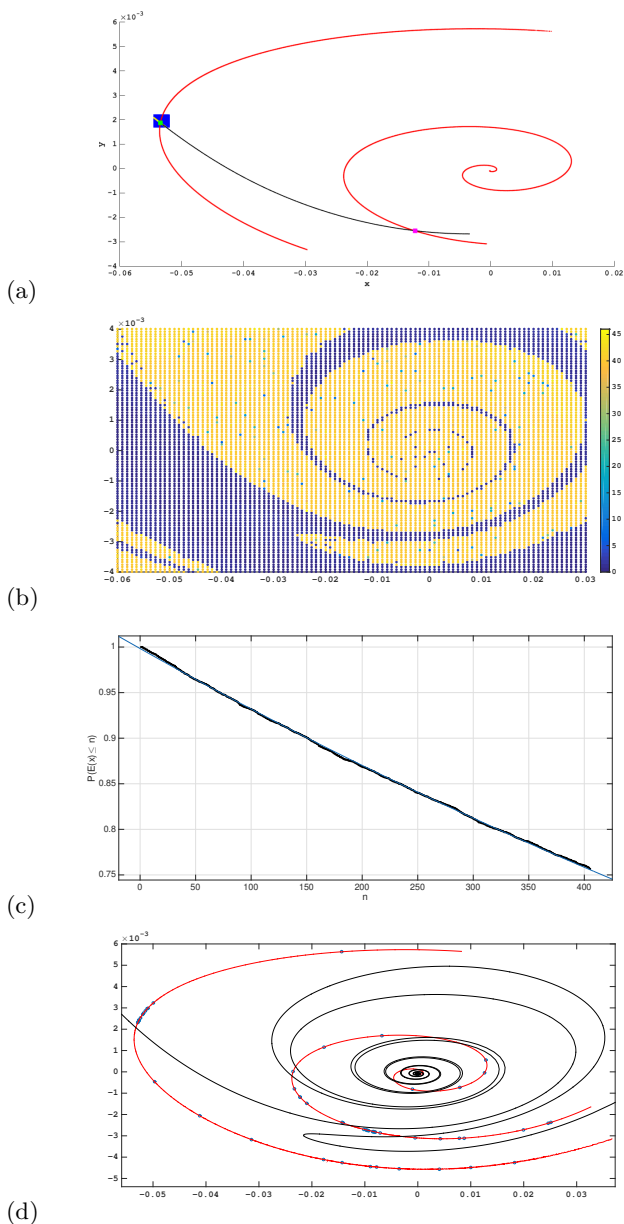


FIG. 12. (a) A saddle equilibrium (green point) of the return map defined on $\Sigma_0 = \{z = 0\}$, together with a neighborhood U (blue grid), image $R(U)$ (red), subset of preimage $U \cap R^{-1}(U)$ (yellow), and a branch of its stable manifold $W^s(p)$ (black). The intersection of $R(U)$ with $W^s(p)$ is also shown (magenta point). (b) Color plot of 10^4 initial conditions beginning in Σ_0 on a 100×100 grid, whose forward trajectories are integrated for the time interval $t \in [0, 600]$. Color denotes number of intersections with Σ_0 with orientation $\dot{z} < 0$. (c) Black points: $P(E(x) \leq n)$ vs. n for 10^4 points sampling a line segment on Σ_+ . Blue curve: least squares exponential fit $y = Ae^{bn}$ of black points, with $A \approx 0.9984$ and $b \approx -6.87 \times 10^{-4}$. (d) Last recorded intersection (blue circles) of each trajectory defined in (b) with Σ_0 . The attracting and repelling spirals (red and black curves, respectively) are overlaid. Parameter set: $\nu \approx 0.00870134$, $a = -0.3$, $b = -1$, $c = 1$.

points x sampling a line segment in Σ_+ , for a very large integration time $t = 2 \times 10^4$. The function $P(E(x) \leq n)$ computes the proportion of those points in the line segment having $E(x) \leq n$. As the sample size grows large, $P(E(x) \leq n)$ converges to the probability that a typical point x (with respect to Lebesgue measure) lies in $R^{-n}(B_0)$. The resulting points admit a fit by an exponential function of the form Ae^{bx} with $b < 0$, suggesting that all points eventually escape with exponential decay. We remind the reader that the one-dimensional approximation $R : \Sigma_+ \rightarrow \Sigma_+$ is given in Fig. 2.

Finally, in Fig. 12(d), we plot the last recorded intersection with Σ_0 of those trajectories that do not tend to Γ within $t = 600$. Even with a relatively sparse grid of 10^4 initial points, these returns sample much of the attracting spiral. Many of the points are not visible at the scale of the figure because they sample the segment shown in Fig. 8(d): the penultimate intersections resulted in the trajectory jumping left to S_ε^{a-} . If a chaotic invariant measure exists, we expect that its support on Σ_0 will be well-approximated by the points given in this figure. In terms of our dynamical partition, the consequence is that we observe arbitrarily long, nonrepeating symbolic sequences consisting of trajectory segments with unpredictable numbers of twists as well as types of twists (due to n , p_{eq} , and Γ).

V. CONCLUDING REMARKS

We have highlighted just a few of the broad range of complex dynamics arising from a tangency of a slow manifold with an unstable manifold of an equilibrium point. This organization is made possible using global bifurcation theory and clever choices of return maps, defined on cross-sections where there is strong contraction near slow manifolds of the system.

We contributed a topological algorithm which classifies trajectories depending on both the number of turns they make, and on the direction of the ‘jump’ toward one of the attracting slow manifolds. This partition gives us some new insight into the way very different turning mechanisms—in this case, a saddle-focus equilibrium point and a folded singularity—interact in a slow-fast system. We used this partition to describe varying types of MMOs with oscillations arising from either of these turning mechanisms, or a combination of both. This demystifies how oscillations of varying types, such as those seen in Fig. 2(c)-(d), may be concatenated in a constructive way to produce MMOs. However, a shortcoming of this analysis is that the partition must be redrawn and reanalyzed for any new parameter set. It is desirable to find a rigorous model which extends trajectories from flow maps defined near cylindrical cross-sections¹⁴ near a saddle-focus equilibrium point, to regions near a folded singularity (one such analysis is provided by Krupa and Wechselberger¹³). Such an extension remains elusive and

is the topic of future work.

We also motivate the study of maps having the topology shown in Fig. 2(a)-(b). These maps are distinguished by two significant features: they admit small disjoint escape subsets, and they may be approximated by unimodal maps over a large proportion of their domains. Sections III B and III C can then be regarded retrospectively as an introduction to the dynamics of these maps, framed in comparison to the relatively well-studied dynamics of unimodal and expansive maps. In particular, such maps undergo period-doubling cascades (Fig. 4) as a system parameter is varied. The forward trajectory of the critical point is also seen to have a transient density for a range of parameters (Fig. 5).

These results lead us to conjecture that statistical properties and universal cascades found in some subfamilies of unimodal maps, such as the quadratic family, persist for the family of maps studied in this paper. The geometric theory of rank-one maps pioneered by Wang and Young²³ is a possible starting point to prove theorems in this direction. This theory has been used successfully to identify chaotic attractors in families of slow-fast vector fields with one fast and two slow variables.²⁴ Their technique is based upon approximating returns by one-dimensional maps.

ACKNOWLEDGMENTS

This work was supported by the National Science Foundation (Grant No. 1006272). The author thanks John Guckenheimer for useful discussions.

¹N. Fenichel, “Persistence and smoothness of invariant manifolds for flows,” *Indiana Univ. Math. J.* **21**, 193–226 (1972).

²J. Guckenheimer, “Singular Hopf bifurcation in systems with two slow variables,” *SIAM J. Appl. Dyn. Syst.* **7**, 1355–1377 (2008).

³J. Guckenheimer, “Return maps of folded node and folded saddle-nodes,” *Chaos* **015108** (2008).

⁴E. Benoît, “Canards et enlacements,” *Inst. Hautes Études Sci. Publ. Math* **72**, 63–91 (1990).

⁵M. Wechselberger, “Existence and bifurcation of canards in \mathbb{R}^3 in

the case of a folded node,” *SIAM J. Appl. Dyn. Syst.* **4**, 101–139 (2005).

⁶M. T. M. Koper and P. Gaspard, “The modeling of mixed-mode and chaotic oscillations in electrochemical systems,” *J. Chem. Phys.* **96**, 7797–7813 (1992).

⁷J. Guckenheimer and I. Lizarraga, “Shilnikov bifurcation of mixed-mode oscillations,” *SIAM J. Appl. Dyn. Syst.* **14**, 764–786 (2015).

⁸J. Guckenheimer and P. Meerkamp, “Unfoldings of singular Hopf bifurcation,” *SIAM J. Appl. Dyn. Syst.* **11**, 1325–1359 (2012).

⁹B. Braaksma, “Singular Hopf bifurcation in systems with fast and slow variables,” *J. Nonlinear Sci.* **8**, 459–490 (1998).

¹⁰J. Guckenheimer and H. Osinga, “The singular limit of a Hopf bifurcation,” *Discrete Cont. Dyn. Syst.* **32**, 2805–2823 (2012).

¹¹C. Jones and N. Kopell, “Tracking invariant manifolds with differential forms in singularly perturbed systems,” *J. Differential Equations* **108**, 64–88 (1994).

¹²C. Jones, “Geometric singular perturbation theory,” (Springer, Berlin, Heidelberg, 1995).

¹³M. Krupa and M. Wechselberger, “Local analysis near a folded saddle-node singularity,” *J. Differential Equations* **248**, 2841–2888 (2010).

¹⁴P. Glendinning and C. Sparrow, “Local and global behavior near homoclinic orbits,” *J. Stat. Phys.* **35**, 645–696 (1984).

¹⁵L. P. Šilnikov, “A case of the existence of a denumerable set of periodic motions,” *Sov. Math. Dokl.* **6**, 163–166 (1965).

¹⁶G. Birkhoff, “Nouvelles recherches sur les systèmes dynamiques,” in *Collected Mathematical Papers, Vol. 2* (Amer. Math. Soc., Providence, R.I., 1950) pp. 530–662.

¹⁷S. Smale, “Diffeomorphisms with many periodic points,” (Princeton Univ. Press, Princeton, N.J., 1965) pp. 63–80.

¹⁸J. Guckenheimer and P. Holmes, “Nonlinear oscillations, dynamical systems, and bifurcations of vector fields,” (Springer-Verlag, Berlin, New York, 1983).

¹⁹G. Pianigiani and J. Yorke, “Expanding maps on sets which are almost invariant: decay and chaos,” *Trans. AMS* **252**, 351–366 (1979).

²⁰M. J. Feigenbaum, “Quantitative universality for a class of nonlinear transformations,” *J. Stat. Phys.* **19**, 25–52 (1978).

²¹P. Couillet and C. Tresser, “Itérations d’endomorphismes et groupe de renormalisation,” *J. Physique* **8**, C5–25 (1978).

²²M. V. Jakobson, “Absolutely continuous invariant measures for one-parameter families of one-dimensional maps,” *Comm. Math. Phys.* **81**, 39–88 (1981).

²³Q. Wang and L.-S. Young, “Toward a theory of rank one attractors,” *Ann. Math.* **167**, 349–480 (2008).

²⁴M. Wechselberger, J. Guckenheimer and L.-S. Young, “Chaotic attractors of relaxation oscillators,” *Nonlinearity* **19**, 701–720 (2006).